Available online at www.eccomasproceedia.org
Eccomas Proceedia COMPDYN (2025) 4502-451

ECCOMAS
Proceedia

COMPDYN 2025
10th ECCOMAS Thematic Conference on
Computational Methods in Structural Dynamics and Earthquake Engineering
M. Papadrakakis, M. Fragiadakis (eds.)
Rhodes Island, Greece, 15-18 June 2025

SEISMIC RESPONSE PREDICTION OF ELECTRICAL EQUIPMENT IN SUBSTATION USING MACHINE LEARNING CHAIN MODELS

Wang Zhu[1,*], Fabrizio Paolacci[2], Gianluca Quinci[2], Qiang Xie[1]

[1]Department of Structural Engineering, Tongji University
Siping Road 1239, Yangpu District, Shanghai, 200092, China
wang4027146@foxmail.com, qxie@tongji.edu.cn

[2]Department of Civil, Computer Science and Aeronautical Technologies Engineering, Roma Tre University
Via Vito Volterra 62, 00146, Rome, Italy
fabrizio.paolacci@uniroma3.it, gianluca.quinci@uniroma3.it

Abstract

Electrical equipment in substations often exhibits multiple potential vulnerable positions during earthquakes, involving insulators and connection flanges. This work proposes a type of machine learning (ML) chain model, where multiple individual models are linked end to end, to predict multiple peak seismic responses of substation equipment at the same time using intensity measures (IMs). In the ML model, the input of the next individual model is combined by IMs and the previous output. The training of ML chain model is presented by bio-inspired multi-objective optimization techniques for the hyperparameters of multiple individual ML models. A case study on a 1100 kV transformer bushing is then conducted. Artificial neural network-kernel ridge regression chain model is established for predicting the peak stresses at two most vulnerable positions. Shaking table tests were performed to validate the accuracy of the proposed ML chain model. Both the evaluation indicators and shaking table tests show enough prediction accuracy. The ML chain model is adept in detecting early damage to electrical equipment, which may aid in post-earthquake quick assessment and relief efforts.

Keywords: Electrical equipment, Substation, Seismic response prediction; Transformer bushing, Machine learning, Shaking table tests.

doi: 10.7712/120125.12752.26125

1 INTRODUCTION

Electrical equipment in substations is critical to the stability and reliability of power systems. However, past major earthquakes have exposed their high seismic vulnerability, often triggering widespread power outages [1,2]. To mitigate the risks, extensive research has examined the seismic performance of key components [3,4]—such as transformers [5-7], bushings [8], and circuit breakers [9,10], and other equipment [11-14]—as well as entire substation systems [15, 16]. These studies have identified both individual and coupled equipment as highly fragile under seismic loads and proposed various mitigation strategies [17–22].

Despite this progress, most research has focused on pre-earthquake design and retrofitting. Post-earthquake emergency repair studies remain limited and often lack detailed insight into individual equipment. In practice, predicting peak stress responses at critical locations, such as porcelain insulator bases or connecting flanges, is essential for rapid damage assessment and repair prioritization. Since peak stress is often used as a proxy for damage severity [9,10,17–19], fast and reliable prediction methods are needed.

Although numerical simulations like finite element modeling can provide accurate estimates, their high computational cost limits practical use in time-sensitive scenarios. Therefore, a rapid, low-data solution is necessary. Machine learning (ML), with its fast prediction capabilities, is a promising tool. ML has shown success in structural engineering for estimating seismic responses in buildings, subways, and RC frames [23–26]. However, ML applications in substation equipment remain rare. Most ML models to date are single-output, suited for structures with one dominant damage index (e.g., inter-story drift). Substation equipment has multiple vulnerable points, making single-output models inefficient. Multi-output ML models offer a more practical and faster solution by predicting several peak responses simultaneously, streamlining post-earthquake assessment.

In response to this challenge, this paper focuses on a practical engineering objective: how to efficiently and rapidly predict multiple peak responses of a single piece of substation equipment using just one machine learning model. Furthermore, the study aims to broaden the application scope of ML in earthquake engineering by introducing a ML chain model for multi-response prediction. The structure of the paper is as follows: Section 2 provides a brief overview of damage characteristics in substation electrical equipment; Section 3 details the development process of ML chain model for structural response prediction; Section 4 presents a case study on a typical 1100 kV transformer bushing to demonstrate the methodology; finally, Section 5 validates the proposed ML model through shaking table experiments.

2 SEISMICAL VULNERABLE POSITIONS OF ELECTRICAL EQUIPMENT

Substation electrical equipment generally comprises a steel support frame, an equipment body, and a connecting flange, as seen in power transformers (Figure 1(a)). The body is often made of brittle, linear-elastic materials like porcelain or GFRP, while the flange is typically cast aluminum, which is also brittle [27,28]. These two components are the most seismically vulnerable, leading to predominantly brittle failures during earthquakes.

Figure 1 shows damage to power transformers during the 2022 Luding earthquake in China [1], including fractures at the base of porcelain insulators (Figure 1(c)) and connection flanges (Figure 1(d)). Post-earthquake investigations [1,8] confirm multiple failure modes in substation equipment, with brittle components being especially vulnerable. Due to their critical role in emergency response, peak stress at these weak points, highlighted in codes like GB 50260-2013 [29] and IEEE 693 [30], must be accurately predicted, making multi-point response prediction essential.

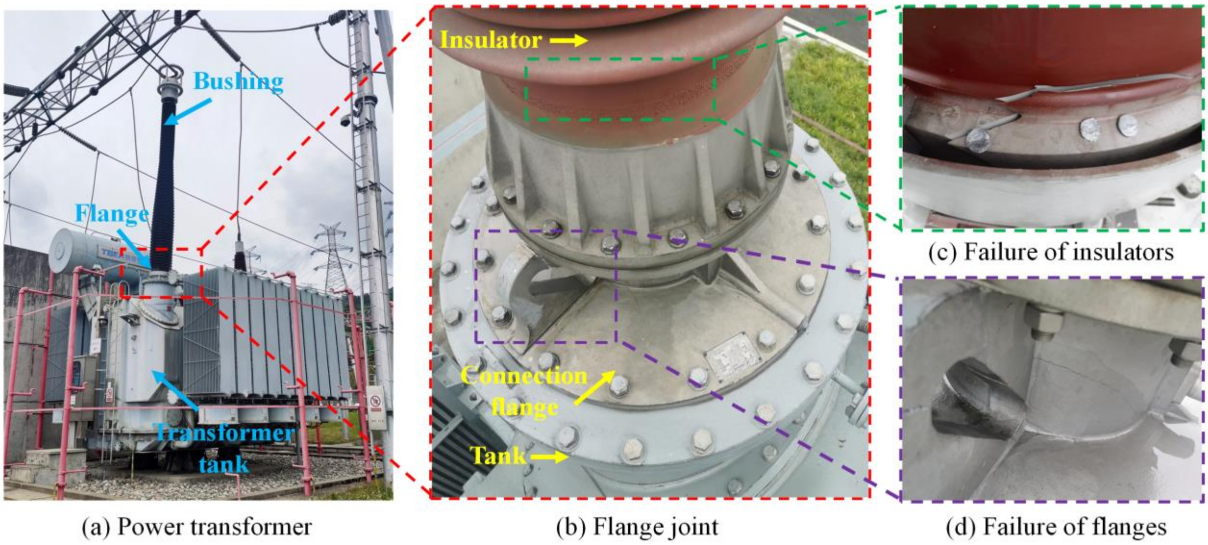

Figure 1: Multiple failure positions of power transformers during the Ms. 6.8 Luding earthquake [1]

3 ML CHAIN MODEL FOR STRUCTURAL MULTI-RESPONSE PREDICTION

3.1 Machine learning chain model

As post-earthquake assessments in substations prioritize peak stress at vulnerable points, this study uses peak stress as the prediction target. This aligns with the linear-elastic behavior of brittle components like porcelain and cast aluminum, unlike ductile structures that rely on deformation-based indices. Supported by ASCE/SEI 43-05 [31], this approach uses ground motion intensity measures (IMs) as inputs, which simplify modeling while maintaining high prediction accuracy.

The input of the prediction model can be expressed as (IM_1, IM_2, IM_3, …, IM_q), where q represents the number of the IMs. For a piece of substation equipment, we can determine its k vulnerable positions that needs to be predicted by simulation or experience. Their peak stress responses are considered as the model output as (O^1, O^2, O^3, …O^k), in which, O^j represents the j-th outputted peak stress (j=1, 2, 3, …, k). The multiple peak responses (O^1, O^2, O^3, …O^k) derive from one piece of equipment, thus there exists fixed relationships between these peak responses. If these relationships can be utilised in the model training and running, the repeat training and multiple runs could be avoided. Therefore, a ML chain model for structural multi-response prediction is proposed in Figure 2.

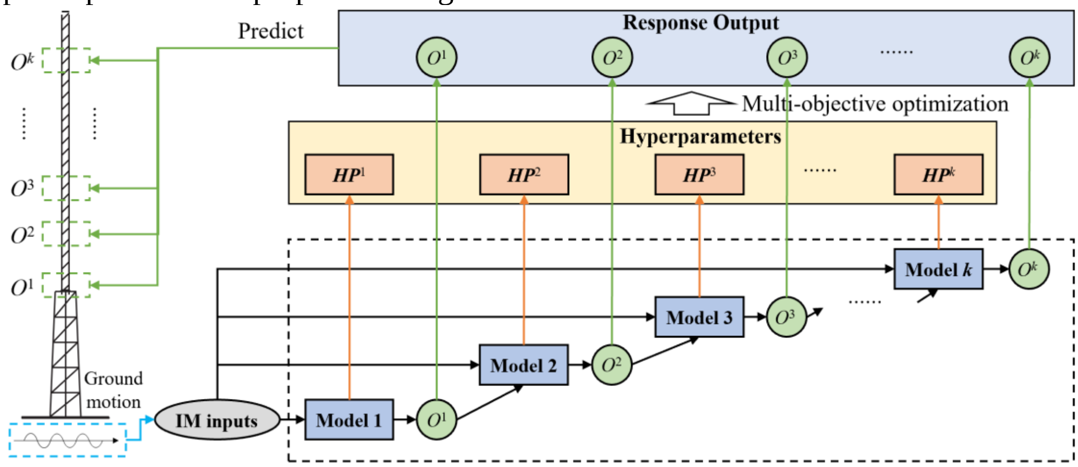

Figure 2: Machine learning chain model for response prediction of substation equipment

It includes a series of single-output ML models linked end to end. Each single-output ML model is in charge of one response output (green part). When training, the first single-output model of each chain model will be established first for the first response O^1. Nevertheless, the second and subsequent models, the model outputs rely on the IMs and the previous model output at the same time, as Eq. (1). Since this chain model considers the IM inputs for each single-output ML model, the ML chain model could acquire more information when trained.

$$O^j = \begin{cases} \boldsymbol{M}^j(IM_1, IM_2, IM_3, ..., IM_q) & j = 1, \\ \boldsymbol{M}^j(IM_1, IM_2, IM_3, ..., IM_q, O^{j-1}) & j = 2, 3, ..., k. \end{cases} \tag{1}$$

3.2 Multi-objective optimization for ML chain model

In theory, the model prediction accuracies for multiple responses (O^1, O^2, O^3, …O^k) should achieve as optimal as possible. Given a prediction evaluation indicator, there would be a group of performance evaluation values (PEVs) for multiple ML models: (PEV^1, PEV^2, PEV^3, …, PEV^k) if the hyperparameters are determined as ($\boldsymbol{HP}^1$, $\boldsymbol{HP}^2$, $\boldsymbol{HP}^3$, …, $\boldsymbol{HP}^k$), in which, $\boldsymbol{HP}^z$ represents a group of hyperparameters for the z-th ML model. Thus, the hyperparameter tuning of the ML chain model can be concluded as a multi-objective optimization problem to be solved as Eq. (2).

$$\begin{cases} \max(PEV^1) = g^1(\boldsymbol{HP}^1, \boldsymbol{HP}^2, ..., \boldsymbol{HP}^k) \\ \max(PEV^2) = g^2(\boldsymbol{HP}^1, \boldsymbol{HP}^2, ..., \boldsymbol{HP}^k) \\ \qquad\qquad\vdots \\ \max(PEV^k) = g^k(\boldsymbol{HP}^1, \boldsymbol{HP}^2, ..., \boldsymbol{HP}^k) \end{cases} \tag{2}$$

where g^j represents the performance evaluation function (PEF) of the j-th ML model based on the given hyperparameter vector ($\boldsymbol{HP}^1$, $\boldsymbol{HP}^2$, …, $\boldsymbol{HP}^k$). Solving this multi-objective optimization problem, the optimal hyperparameters can be obtained for the ML chain model, with an overall optimal prediction accuracy.

4 CASE STUDY ON A 1100 KV TRANSFORMER BUSHING

4.1 Structural components and FE simulation model

To illustrate the application of the proposed ML chain model, a 1100 kV porcelain transformer bushing is used as a case study. In practice, it is mounted on a transformer tank, but due to the tank's size and weight, tests typically use a rigid steel frame instead [30]. This study follows that approach, selecting a bushing-frame system (Figure 3(a)). The frame, with a simulated natural frequency of 40.57 Hz, which is above the 33 Hz minimum in IEEE 693 std, is considered rigid. The bushing is fixed to the top plate via its connection flange.

The main components of the bushing are shown in Figure 3(b). The air-side porcelain insulator has a bottom outer diameter of 640 mm and an inner diameter of 550 mm, tapering to a minimum outer diameter of 390 mm near the top. The insulator is 10.182 m long, with the full bushing length reaching 13 m. An aluminum-core conductor runs through the center. The mass center of the air-side insulator is 4.645 m above the flange, while the bushing's overall center of mass is 4.070 m high. The air-side portion weighs 5073 kg, the total bushing weighs 7135 kg, and the steel frame weighs 2891 kg.

The FE model of the 1100 kV bushing was built in ABAQUS. S4R shell elements modeled the corona rings, bushing stiffeners, and frame top plate, while B31 beam elements represented the frame brackets. All other components used C3D8R solid elements. The air-side insulator excluded the effect of umbrellas and focused on bulk properties. A 10-mm cement layer was added at the base of the insulator to account for rotational stiffness. Material properties included: porcelain (E = 106 GPa, ν = 0.25) and cast aluminum flange (E = 60 GPa, ν = 0.3). The coordinate system is shown in Figure 3(a).

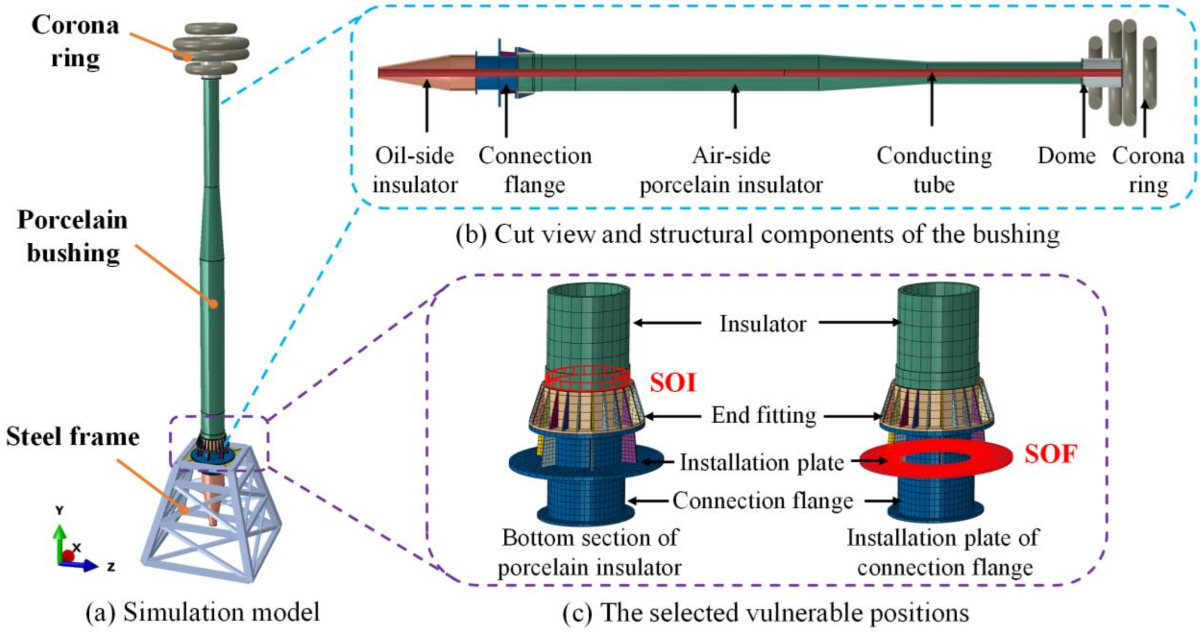

Figure 3. FE simulation model of the 1100 kV transformer bushing and vulnerable positions

4.2 Selection of natural ground motions

Given the axisymmetric nature of the transformer-bushing system, horizontal ground motion input in a single direction is sufficient, as permitted by IEEE 693 std [30]. In this study, the X-axis is selected as the input direction. To ensure the ML chain model is trained on a wide range of seismic scenarios, a large and diverse set of ground motions is required.

Considering the site conditions (soil Type 2), 500 ground motions were initially selected from the PEER database, based on Vs30 values between 265 and 550 m/s. Since strong motions are underrepresented in the database, a scaling strategy was applied to enhance the intensity variation. This process discretized the peak ground acceleration (PGA) levels, ultimately generating 2550 ground motions. The resulting dataset covers a wide spectrum, with PGA values ranging from 0 to 1.4 g and spectral accelerations $S_a(2\%, T_1)$ from 0 to 5.1 g, providing sufficient diversity for robust model training.

4.3 Acquisition and analysis of sample data

Because ground motions will be input into the FE model, their intensity measures (IMs) are extracted. While numerous IMs exist, no consensus has been reached on which best correlate with structural response [32]. IMs are typically categorized as amplitude-dependent (e.g., PGA), duration-dependent (e.g., energy duration), or spectrum-dependent (e.g., $S_a(2\%, T_1)$). This study selects ten widely used IMs covering all three types (Table 1). Except for $S_a(2\%, T_1)$, which is structure-specific, most IMs are structure-independent to enhance generality.

The proposed ML chain model can predict multiple failure modes for a single piece of equipment using these IM data. In this case study, the bushing, a representative porcelain cylindrical component, has two vulnerable positions: the bottom cross section of the insulator and the installation plate of the connection flange (Figure 3(c)). These are denoted as SOI (Stress of insulator) and SOF (Stress of flange), respectively. Therefore, the output of the ML chain model is SOI and SOF.

Table 1: Selected ground motion parameters (IMs) and categories

No.	IM	Abridged notation	Category
1	Peak ground acceleration	PGA	Amplitude-dependent type
2	Peak ground velocity	PGV	
3	Peak ground displacement	PGD	
4	Root mean square of acceleration	RMS_a	
5	Standard cumulative absolute velocity	CAV_{std}	
6	Arias intensity	I_a	
7	Strong motion duration (90% energy duration)	t_e	Duration-dependent type
8	Maximum dynamic coefficient	β_{max}	Spectrum-dependent type
9	Period corresponding to the peak acceleration response spectrum	T_{peak}	
10	Spectral acceleration at the fundamental period	$S_a(2\%,T_1)$	

4.4 ML Chain model

To establish the ML chain model, the basic ML models should be determined first. This study selects eight widely used ML algorithms and then determines the optimal as the basic ML models. The eight ML algorithms include kernel ridge regression (KRR), support vector regression (SVR), k-nearest neighbour (KNN), decision tree regression (DTR), gradient boosting regression (GBR), Adaptive boosting (ADAboost), Random forest (RF) and artificial neural network (ANN). All of them are well-known algorithms but are not the focus in this study, thus their introductions were neglected.

To evaluate the model accuracy, two evaluation indicators, root mean squared error (RMSE) and coefficient of determination (R^2), were selected to compare the errors between the prediction results and the simulation results, as shown in Eqs. (3) and (4).

$$\mathrm{RMSE} = \sqrt{\sum_i (y_i - \hat{y}_i)^2 / n} \tag{3}$$

$$R^2 = 1 - \sum_i (y_i - \hat{y}_i)^2 / \sum_i (y_i - \bar{y})^2 \tag{4}$$

In which, y_i and $\bar{y}$ are the peak stress responses of the FE model and their average value, respectively, $\hat{y}_i$ is the prediction response of the ML model, n is the total number of the testing samples. The ML chain model involves two mapping relationships: IMs to SOI, and IMs + SOI to SOF. The first 2000 samples (80%) are used for training, with the remaining 20% for testing. After training with various hyperparameter ranges, the optimal models, based on the highest R^2 and lowest RMSE, are determined to be ANN and KRR. Using ANN and KRR, a ML chain model is built as Figure 4.

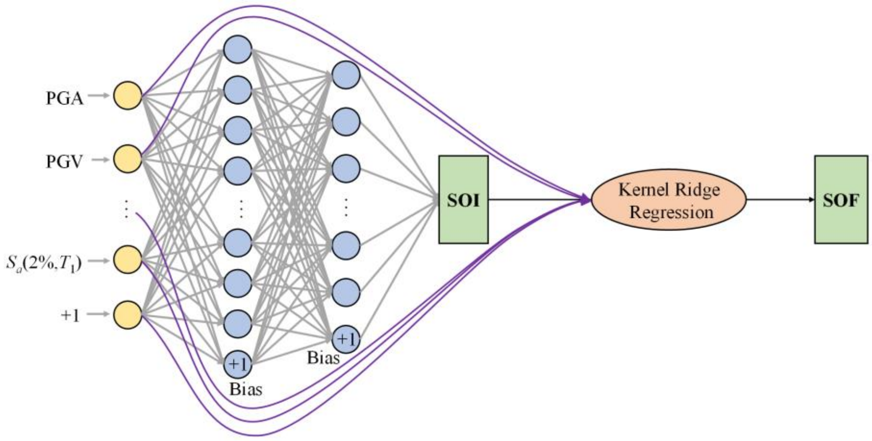

Figure 4. ML chain model for the 1100 kV transformer bushing

4.5 Training and multi-objective optimization

As previously mentioned, the ML chain model requires optimization of three hyperparameters: (NN_1, NN_2) for ANN and the regularization coefficient α for the KRR model. Different hyperparameter combinations lead to varying prediction performances, impacting evaluation indices such as R^2 for SOI and SOF. To optimize these indices, the hyperparameters are tuned to achieve better prediction results, as outlined in Eq. (5).

$$\begin{cases} \max(\mathrm{R}_1^2) = g^1(NN_1, NN_2, \alpha) \\ \max(\mathrm{R}_2^2) = g^2(NN_1, NN_2, \alpha) \end{cases} \tag{5}$$

where R_1^2 and R_2^2 represent the R^2 for SOI and SOF prediction results, respectively. Therefore, the main task for the model refinement is to solve the objective functions Eq. (5), making SOI and SOF predictions more accurate at the same time.

Multi-objective optimization of the ML chain model hyperparameters was performed using NSGA-II, a bio-inspired evolutionary algorithm for efficient multi-objective optimization. The search ranges for NN1, NN2, and α were set as 1-200, 1-200, and 0.001-1000, respectively. The optimization involved 50 particles and 1500 iterations. As generations progressed, the non-dominated points were updated, resulting in a Pareto front. Based on equal importance for SOI and SOF, the optimal hyperparameters from the final generation were NN_1=175, NN_2=187, and α=851.6, yielding R^2(SOI)=0.975 and R^2(SOF)=0.946.

5 SHAKING TABLE TESTS AND VALIDATION

5.1 Experimental installation and input

The shaking table tests were conducted at Tongji University's multifunctional lab [8], with the transformer bushing installed on a steel frame, as shown in Figure 5(a–b). The assembly was anchored to the shaking table via bolts at the frame base, where ground motions were applied. The model's dimensions matched the FE model exactly (Figure 5(c)).

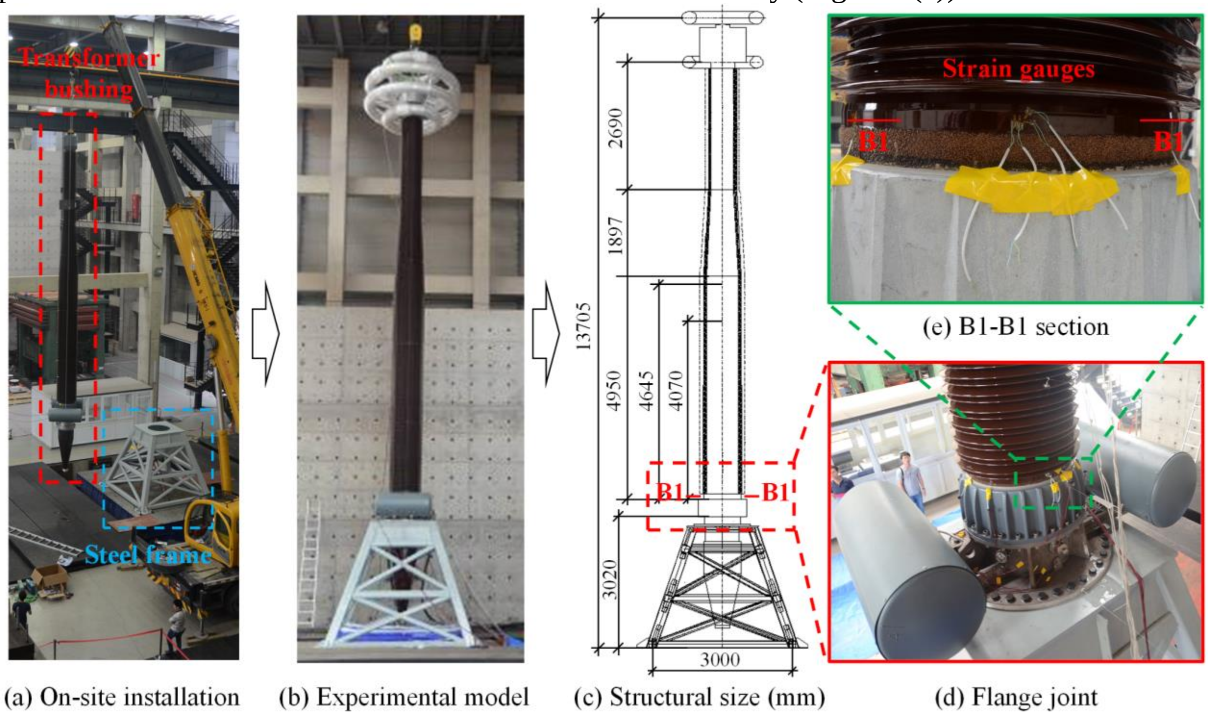

Figure 5: Shaking table tests of transformer bushing and sensor installation

Strain gauges were installed at key locations, including the flange joint and the bottom section of the porcelain insulator (B1–B1), as illustrated in Figure 5(d–e). These gauges recorded strain data, allowing calculation of peak stress via elastic modulus, which was then used to validate the ML-predicted SOI. There were not sensors for flanges, but visible flange damage during tests provided valuable validation for the predicted SOF.

The experiment used a single-directional input, with an artificial ground motion selected to match the required response spectrum (RRS) as per the relevant code [34]. The standardized acceleration time history and its response spectrum are shown in Figure 6, demonstrating a good match with the RRS. Based on seismic fortification requirements, the design basic acceleration was 0.3 g, and the target PGA was set at 0.53 g after applying the transformer tank amplification factor and steel frame considerations. The experiment involved two primary ground motion scenarios (TS2 and TS4) and two white noise scenarios for detecting structural health. In total, four test scenarios were conducted, as outlined in Table 2.

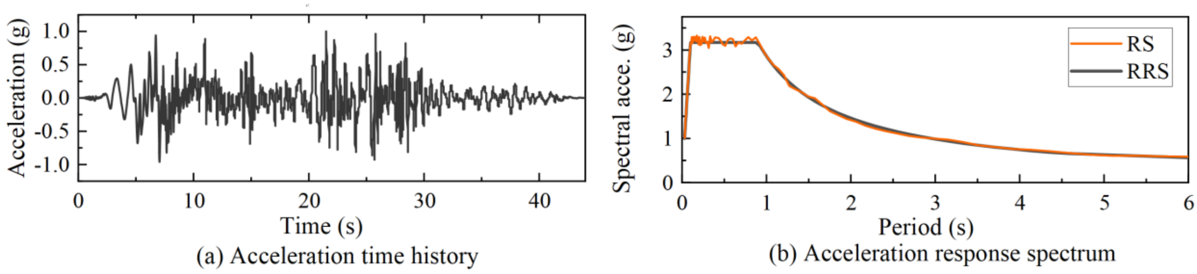

Figure 6: Standardized acceleration time history and RS of the artificial wave

Table 2: Test scenarios of shaking table tests for the transformer bushing

Test scenarios	Earthquake motion	Target PGA/g	Measured PGA/g
TS1	White noise	0.075	0.104
TS2	Artificial ground motion	0.150	0.156
TS3	White noise	0.075	0.104
TS4	Artificial ground motion	0.530	0.620

5.2 Experimental results

The results from TS1 and TS3 showed no damage to the transformer bushing in TS2, while TS4 revealed significant damage, including cracks and oil leakage at the connection flange installation plate (Figure 7). The damage occurred around the sixth second of the artificial wave, with irregular crack propagation, highlighting the challenge of sensor-based monitoring and emphasizing the need for ML response prediction model. The porcelain insulator remained intact in TS4, and its monitoring data were used for validating the ML chain model.

Figure 7: Damage to the transformer bushing in the shaking table tests

5.3 Validation of the ML chain model

To further validate the model performance, calculate the IMs of the excitations in TS2 and TS4, then input them to the ML chain model. The prediction results are provided in Table 3, where the experimental results rely on the strain gauges and the elastic modulus of 106 GPa of porcelain insulators. Meanwhile, the peak responses obtained from the FE model are also provided as a reference.

In TS2, the ML chain model accurately predicted the SOI with an error of 5.12%, while SOF prediction was consistent with the non-damaged state and FE model. In TS4, predicted SOF value was close to the material strength of the flange, matching the observed damage. However, the predicted SOI in TS4 deviated from experimental results because the ML model, trained with undamaged data, predicted whole time history responses, while the experiment recorded peak responses at the flange fracture. Despite this, the small errors demonstrate the good prediction accuracy. The ML chain model is effective for detecting early structural damage, though not for continuous destruction. They help identify damaged equipment post-earthquake, enabling rapid decisions and improving substation resilience.

Table 3: Comparison of predicted and experimental results in TS2 and TS4 (Unit: MPa)

Model	TS2		TS4	
	SOI	SOF	SOI	SOF
Experiment model	10.262	Non-damaged	14.570*	Damaged
FE model	10.527 (2.58% error)	54.311 (consistent)	41.827** (inconsistent)	215.794 (consistent)
ML chain model	10.787 (5.12% error)	55.702 (consistent)	42.952 (inconsistent)	215.290 (consistent)

Note: * The value is obtained from the recorded data at and before the failure time moment.
** The value is obtained from the FE model during the whole time history.

6 CONCLUSIONS

This paper proposes a chain model to predict multiple peak seismic responses of one piece of equipment using IMs. Then, a case study on a 1100 kV transformer bushing is performed to validate the feasibility. The conclusions are as follows:

(1) In the case study, ANN-KRR chain model is established and optimized using NSGA-II optimization algorithm, whose effectiveness and feasibility are validated by both evaluation indicators and shaking table tests.
(2) ML chain model shows high computational efficiencies in both pre-earthquake training phase and post-earthquake running phase. They avoid pre-earthquake repeated trainings for multiple single ML models and post-earthquake time history calculations.
(3) The ML chain model is mainly qualified for finding the earliest damage to substation equipment. This capability is valuable for identifying damaged equipment after earthquakes within a short time, further assisting post-earthquake rapid decisions.

REFERENCES

[1] W. Zhu, Q. Xie, X. Liu, B. Mao, Z. Xue, Towards 500 kV power transformers damaged in the 2022 Luding earthquake: Field investigation, failure analysis, and seismic retrofitting, *Natural Hazards*, **120**, 6275-6305, 2024.

[2] E. Fujisaki, S. Takhirov, Q. Xie, K.M. Mosalam, Seismic vulnerability of power supply: Lessons learned from recent earthquakes and future horizons of research, *9th International Conference on Structural Dynamics*, pp. 345-350, Porto, Portugal, n.d.

[3] Y. Xue, Y. Cheng, Z. Zhu, S. Li, Z. Liu, H. Guo, S. Zhang, Study on seismic performance of porcelain pillar electrical equipment based on nonlinear dynamic theory, *Advances in Civil Engineering*, **2021**, 1-17, 2021.

[4] W. Zhu, M. Wu, Q. Xie, J. Xu, Floor response spectra and seismic design method of electrical equipment installed on floor in indoor substation, *Soil Dynamics and Earthquake Engineering*, **173**, 108138, 2023.

[5] X. Li, Q. Xie, J. Wen, Double friction pendulum-based isolation optimization for transformer-bushing systems, *Engineering Structures*, **320**, 118909, 2024.

[6] M. Wang, J. He, Shake table test and finite element model for evaluating seismic performance of 220 kV transformer-bushing systems, *Earthquake Spectra*, 87552930231177089, 2023.

[7] W. Zhu, X. Bian, Q. Xie, Refined seismic fragility curves of substation equipment considering ground motion classifications, *Soil Dynamics and Earthquake Engineering*, **187**, 108995, 2024.

[8] C. He, Q. Xie, Y. Zhou, Influence of flange on seismic performance of 1,100-kV ultra-high voltage transformer bushing, *Earthquake Spectra*, **35(1)**, 447-469, 2019.

[9] S. Alessandri, R. Giannini, F. Paolacci, M. Malena, Seismic retrofitting of an HV circuit breaker using base isolation with wire ropes. Part 1: Preliminary tests and analyses, *Engineering Structures*, **98**, 251-262, 2015.

[10] S. Alessandri, R. Giannini, F. Paolacci, M. Amoretti, A. Freddo, Seismic retrofitting of an HV circuit breaker using base isolation with wire ropes. Part 2: Shaking-table test validation, *Engineering Structures*, **98**, 263-274, 2015.

[11] A. S. Whittaker, G. L. Fenves, A. S. J. Gilani, Seismic evaluation and analysis of high-voltage substation disconnect switches, *Engineering Structures*, **29(12)**, 3538-3549, 2007.

[12] W. Zhu, F. Paolacci, G. Quinci, Q. Xie, A novel approach for seismic risk assessment of porcelain cylindrical electrical equipment, *International Journal of Disaster Risk Reduction*, **124**, 105524, 2025.

[13] C. He, Z. He, W. Zhu, Seismic interconnecting effects of multi-span flexible conductor-post electrical equipment coupling system, *Journal of Constructional Steel Research*, **212**, 108209, 2024.

[14] G. Quinci, C. Nardin, F. Paolacci, O. S. Bursi, Modelling of non-structural components of an industrial multi-storey frame for seismic risk assessment, *Bulletin of Earthquake Engineering*, **21**, 6065-6089, 2023.

[15] W. Zhu, Q. Xie, Post-earthquake rapid assessment for loop system in substation using ground motion signals, *Mechanical Systems and Signal Processing*, 208, 111058, 2024.

[16] J. Lu, Q. Xie, W. Zhu, Seismic damage detection of ultra-high voltage transformer bushings using output-only acceleration responses, *Journal of Civil Structural Health Monitoring*, **13**, 1091-1104, 2023.

[17] W. Bai, M.A. Mohamed, J.W. Dai, Seismic fragilities of high-voltage substation disconnect switches, *Earthquake Spectra*, **35(4)**, 1559-1582, 2019.

[18] C. He, L.Z. Jiang, L.Q. Jiang, Seismic failure risk assessment of post electrical equipment on supporting structures, *IEEE Transactions on Power Delivery*, **38(4)**, 2757-2766, 2023.

[19] F. Paolacci, R. Giannini, D. Phan Hoang Nam, D. Corritore, G. Quinci, Scores: An algorithm for records selection to employ in seismic risk and resilience analysis, *Procedia Structural Integrity*, **44**, 307-314, 2023.

[20] W. Bai, M.A. Mohamed, J.W. Dai, Seismic response of potential transformers and mitigation using innovative multiple tuned mass dampers, *Engineering Structures*, **174**, 67-80, 2018.

[21] W. Bai, J.W. Dai, H.M. Zhou, Y.Q. Yang, X.Q. Ning, Experimental and analytical studies on multiple tuned mass dampers for seismic protection of porcelain electrical equipment, *Earthquake Engineering and Engineering Vibration*, **16**, 803-813, 2017.

[22] W. Bai, W. Zhu, M.A. Moustafa, J.W. Dai, Seismic mitigation of porcelain cylindrical electrical equipment using synergistic concept with base isolation and tuned mass damper, *Earthquake Spectra*, 87552930241287005, 2024.

[23] G. Quinci, N. H. Phan, F. Paolacci, On the use of artificial neural network technique for seismic fragility analysis of a three-dimensional industrial frame, *Proceedings of the ASME Nondestructive Evaluation, Diagnosis and Prognosis Division (NDPD)*, Las Vegas, Nevada, USA, 2022.

[24] G. Quinci, F. Paolacci, M. Fragiadakis, O. S. Bursi, A machine learning framework for seismic risk assessment of industrial equipment, *Reliability Engineering & System Safety*, **254**, 110606, 2025.

[25] W. Zhu, Q. Xie, Machine learning chain models for multi-response prediction of electrical equipment in substation subjected to earthquakes, *Engineering Structures*, **319**, 118815, 2024.

[26] F. Kazemi, N. Asgarkhani, R. Jankowski, Machine learning-based seismic response and performance assessment of reinforced concrete buildings, *Archives of Civil and Mechanical Engineering*, **23(2)**, 94, 2023.

[27] S.S. Scherrer, U. Lohbauer, A. Della Bona, et al., ADM guidance-Ceramics: Guidance to the use of fractography in failure analysis of brittle materials, *Dental Materials*, **33(6)**, 599-620, 2017.

[28] B. Defez, G. Peris-Fajarnés, V. Santiago, J.M. Soria, E. Lluna, Influence of the load application rate and the statistical model for brittle failure on the bending strength of extruded ceramic tiles, *Ceramics International*, **39(3)**, 3329-3335, 2013.

[29] GB 50260-2013, Code for seismic design of electrical installation, 2013.

[30] IEEE Std 693-2018, IEEE recommended practice for seismic design of substations, 2018.

[31] J. I. Braverman, J. Xu, B. R. Ellingwood, C.J. Costantino, R.J. Morante, C.H. Hofmayer, Evaluation of the seismic design criteria in ASCE/SEI standard 43-05 for application to nuclear power plants, *US Nuclear Regulatory Commission*, Job Code N, 1-73, 2007.

[32] L. Ye, Q. Ma, Z. Miao, H. Guan, Y. Zhuge, Numerical and comparative study of earthquake intensity indices in seismic analysis, *The Structural Design of Tall and Special Buildings*, **22(4)**, 362-381, 2013.

[33] K. Deb, A. Pratap, S. Agarwal, T.A.M.T. Meyarivan, A fast and elitist multiobjective genetic algorithm: NSGA-II, *IEEE Transactions on Evolutionary Computation*, **6(2)**, 182-197, 2002.

[34] State Grid Corporation of China (SGCC), Technical specification for seismic design of ultra-high voltage porcelain insulating equipment and installation/maintenance to energy dissipation devices (Q/GDW11132-2013), Beijing, 2014.